Probing dark excitons in atomically thin semiconductors via near-field coupling to surface plasmon polaritons

You Zhou[1,2†], Giovanni Scuri[2†], Dominik S. Wild[2†], Alexander A. High[1,2†], Alan Dibos[1], Luis A. Jauregui[2], Chi Shu[2], Kristiaan De Greve[1,2], Kateryna Pistunova[2], Andrew Y. Joe[2], Takashi Taniguchi[3], Kenji Watanabe[3], Philip Kim[2*], Mikhail D. Lukin[2*] and Hongkun Park[1,2*]

Transition metal dichalcogenide (TMD) monolayers with a direct bandgap feature tightly bound excitons, strong spin–orbit coupling and spin–valley degrees of freedom[1-4]. Depending on the spin configuration of the electron–hole pairs, intra-valley excitons of TMD monolayers can be either optically bright or dark[5-8]. Dark excitons involve nominally spin-forbidden optical transitions with a zero in-plane transition dipole moment[9], making their detection with conventional far-field optical techniques challenging. Here, we introduce a method for probing the optical properties of two-dimensional materials via near-field coupling to surface plasmon polaritons (SPPs). This coupling selectively enhances optical transitions with dipole moments normal to the two-dimensional plane, enabling direct detection of dark excitons in TMD monolayers. When a WSe_2 monolayer is placed on top of a single-crystal silver film[10], its emission into near-field-coupled SPPs displays new spectral features whose energies and dipole orientations are consistent with dark neutral and charged excitons. The SPP-based near-field spectroscopy significantly improves experimental capabilities for probing and manipulating exciton dynamics of atomically thin materials, thus opening up new avenues for realizing active metasurfaces and robust optoelectronic systems, with potential applications in information processing and communication[11].

When an optical dipole is in proximity to a metallic substrate, it can emit light into both far-field photons and surface plasmon polaritons (SPPs). Far-field emission can be measured directly via top-down optical microscopy, whereas SPP emission can be detected by converting SPPs into far-field light via engineered out-coupling structures (Fig. 1a). On a single-crystal silver film—our metal of choice due to its low loss[10]—SPPs are strongly polarized in the out-of-plane (z) direction in the visible frequency range (see Supplementary Section I). Consequently, the emission rate into SPPs is much greater for an out-of-plane dipole than for an in-plane dipole (Fig. 1b,c), with the enhancement factor exceeding 30 for the present device parameters (Fig 1d; for details of the analysis see Supplementary Sections II–III). At the same time, far-field emission of an in-plane dipole is strongly suppressed (Fig. 1b,d), because the in-plane electric field is close to zero near the silver surface. We note that when a point dipole is close to a metal[12], non-radiative recombination due to ohmic loss can be the dominant decay mechanism. However, for delocalized excitons in quantum wells[13] and two-dimensional materials, quenching of

exciton luminescence by ohmic loss is significantly reduced, even when they are placed 10 nm above a silver surface (Supplementary Fig. 1 and Supplementary Section III). Combined together, the net effect of a nearby silver surface is significantly enhanced (suppressed) emission of an out-of-plane (in-plane) dipole into SPPs (the far field).

In the present experiment we used exfoliated monolayers of WSe_2 or $MoSe_2$ encapsulated between thin, insulating hexagonal boron nitride (hBN) flakes. The photoluminescence spectra of these heterostructures exhibit narrow excitonic features (linewidths of ~2–4 meV) at 4 K. A transition metal dichalcogenide (TMD) monolayer encapsulated by hBN is placed on atomically smooth single-crystal silver[10]. In our devices, silver plays dual roles: it supports SPPs that can be coupled to TMD excitons and it serves as a gate electrode that can change the electrostatic potential of a TMD monolayer (Fig. 1a). The spacing between the monolayer TMD and the silver surface is determined by the bottom hBN thickness and can easily be controlled by varying this thickness. In our devices, the typical spacing was on the order of 10 nm.

Excitons were created using off-resonant 660 nm laser excitation, and the photoluminescence (PL) spectra were collected either from the same spot excited by the laser via far-field imaging (FF-PL), or from scattered SPPs at the out-coupling structures (SPP-PL, inset of Fig. 1e). At 4 K, the FF-PL spectrum of WSe_2 displays several commonly observed spectral features, assigned previously to neutral exciton emission (X_0), charged exciton emission (X_T) and the lower-energy emission (L1) often attributed to defects[14]. Both X_0 and X_T are known to have only in-plane transition dipole moments[15]. The SPP-PL spectrum, however, exhibits an additional large peak (X_D) at 731 nm that is absent in the far-field spectrum, with a narrower linewidth (~2 meV) than the other spectral features. In contrast, neither the FF-PL nor SPP-PL spectra of monolayer $MoSe_2$ exhibit the feature corresponding to X_D in WSe_2 SPP-PL (Supplementary Fig. 2). These observations suggest that the WSe_2-specific X_D feature is associated with an out-of-plane transition dipole moment that preferentially couples to SPPs.

To further explore the nature of excitonic species in monolayer TMDs, we compared the FF-PL and SPP-PL spectra for monolayer WSe_2 and $MoSe_2$ as we tuned the carrier density by means of a gate voltage. It is well known that the neutral exciton emission (X_0) of TMD monolayers only exists inside the bandgap[16]. Once electrons or holes are added to the conduction band (CB) or valence band (VB) of the TMD monolayers via electrostatic doping by a gate

[1]Department of Chemistry and Chemical Biology, Harvard University, Cambridge, Massachusetts 02138, USA. [2]Department of Physics, Harvard University, Cambridge, Massachusetts 02138, USA. [3]National Institute for Materials Science, 1-1 Namiki, Tsukuba 305-0044, Japan. [†]These authors contributed equally to this work. *e-mail: hongkun_park@harvard.edu; lukin@physics.harvard.edu; pkim@physics.harvard.edu
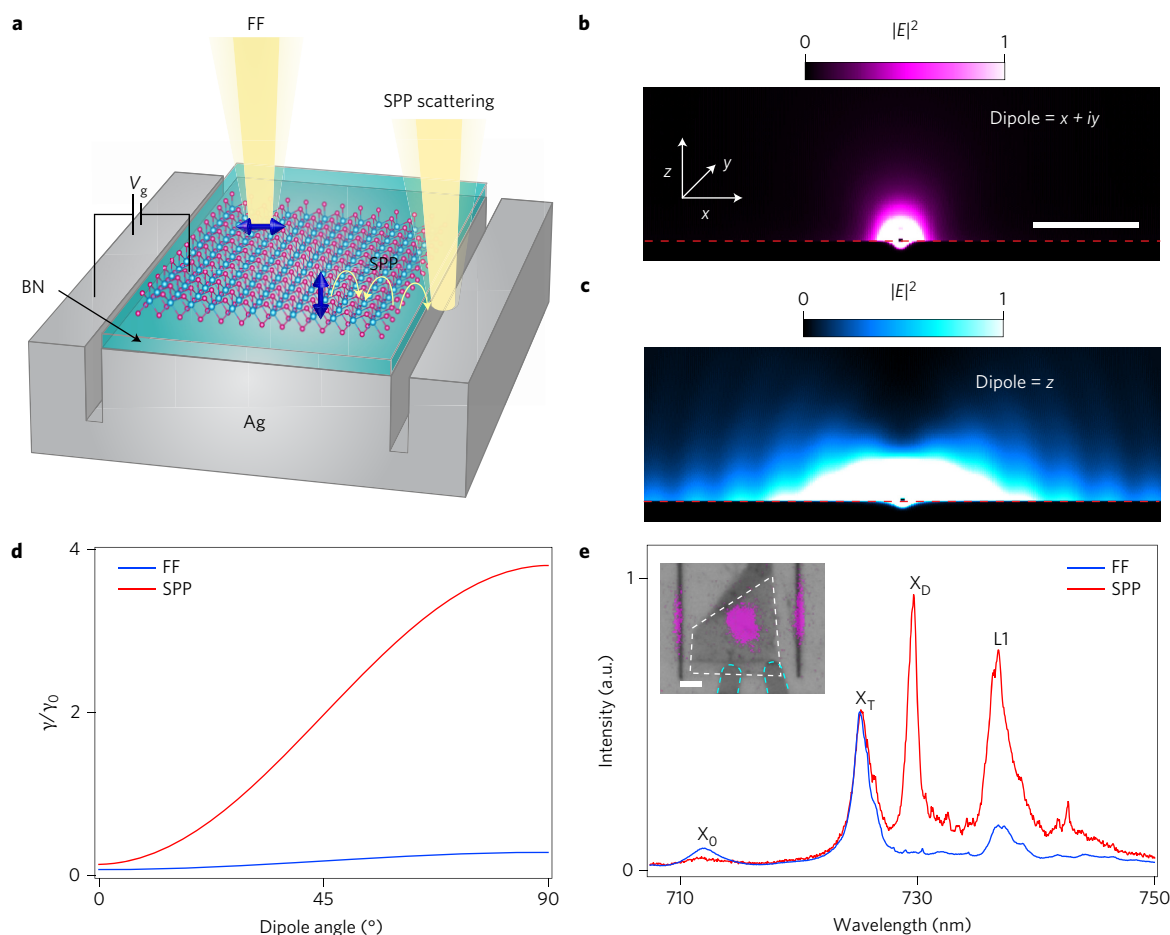
Figure 1 | Probing out-of-plane electric dipole transitions in two-dimensional materials via near-field coupling to SPPs. a, Schematic of the experimental set-up. A TMD-based van der Waals heterostructure is placed on top of single-crystal silver with silver acting as the backgate (V_g). Optical transitions can couple to both near-field SPPs and the far field (FF). Coupling to SPPs can be detected by scattering the SPPs into the FF using nanoscale trenches etched into silver. **b,c**, Finite-difference time-domain simulation of the electric-field intensity radiated by an in-plane point dipole emitter (**b**) and an out-of-plane point dipole emitter (**c**). The emitter is positioned 10 nm above the silver surface. Scale bar, 1 μm. **d**, Emission rate γ into the FF (blue) and SPPs (red) as a function of angle θ between the transition dipole and the two-dimensional plane (0° is defined as in the two-dimensional plane). γ_0 is the decay rate of the exciton population in vacuum at $T = 4$ K. In the analysis, the dipole emitter is 8 nm above a silver film, with 8 nm (5 nm) thick hBN below (above) the dipole to match the heterostructure geometry in the experiment. The emission wavelength is 720 nm. Far-field emission is defined as emission into an objective lens above the sample with numerical aperture of 0.75, to match the experimental measurement geometry. **e**, Photoluminescence spectra of WSe$_2$ collected from the FF (blue) and from scattered SPPs (red) at $T = 4$ K and at zero applied gate voltage, showing the neutral exciton (X_0), charged exciton (X_T) and lower energy (L1) emission. In the SPP scattered spectrum, an additional peak, X_D, is observed. Inset: photoluminescence intensity map with a fixed incident excitation beam overlaid with an optical image of a monolayer WSe$_2$ device on silver. The white dashed (cyan-dashed) line indicates the region of WSe$_2$ (electrical contacts). Scale bar, 1 μm.

voltage, the emission from X_0 vanishes, and the photoluminescence spectra are dominated by the charged exciton emission, X_T. In Fig. 2a–d and in Supplementary Figs 2 and 3, such trends are evidenced by the simultaneous disappearance of X_0 and the onset of in-plane conduction outside the bandgap region (-2.5 V $< V_g < 0$ V)[17]. The gate-dependent SPP-PL spectra of a WSe$_2$ monolayer in Fig. 2b show that emission from X_D exists only within the same voltage range as the bright neutral exciton X_0.

Outside the bandgap region, additional optical transitions with an out-of-plane dipole orientation emerge. Figure 3a,b presents the FF-PL and SPP-PL spectra of WSe$_2$ at different gate voltages. We normalized both FF-PL and SPP-PL spectra using the intensity of a charged exciton peak X_T, because it is known to involve a purely in-plane transition dipole moment[15]. The ratio of SPP-PL intensity to the FF-PL intensity after normalization provides a direct measure of the orientation of the transition dipole for each luminescent species: the unity ratio represents a purely in-plane dipole, and a value larger than one indicates that the transition dipole has some

out-of-plane components. Based on our theoretical calculations presented in Fig. 1d and Supplementary Fig. 4, an optical transition with a purely out-of-plane transition dipole should have a normalized coupling ratio of 7 in our device geometry. The experimental results for X_D yield a value of 16: this discrepancy between theory and experiment is probably due to small, yet non-negligible, absorption of SPPs by charged excitons as they propagate through the WSe$_2$, which increases the apparent coupling ratio of X_D after normalization. Indeed, Supplementary Fig. 5 shows that there can be sizeable absorption of SPPs due to charged excitons when SPPs propagate through several micrometres of the WSe$_2$ channel. When SPPs propagate through a minimal distance (less than 1 μm) within WSe$_2$ (Supplementary Fig. 6), the normalized coupling ratio determined by experiment is close to 7, in good agreement with the theoretical calculations. Figure 3b shows that the value of the normalized coupling ratio in WSe$_2$ is large not only for the neutral exciton peak X_D at 731 nm, but also for the L1 peak at 740 nm. Specifically, in the bandgap region (-2.5 V $< V_g < 0$ V),
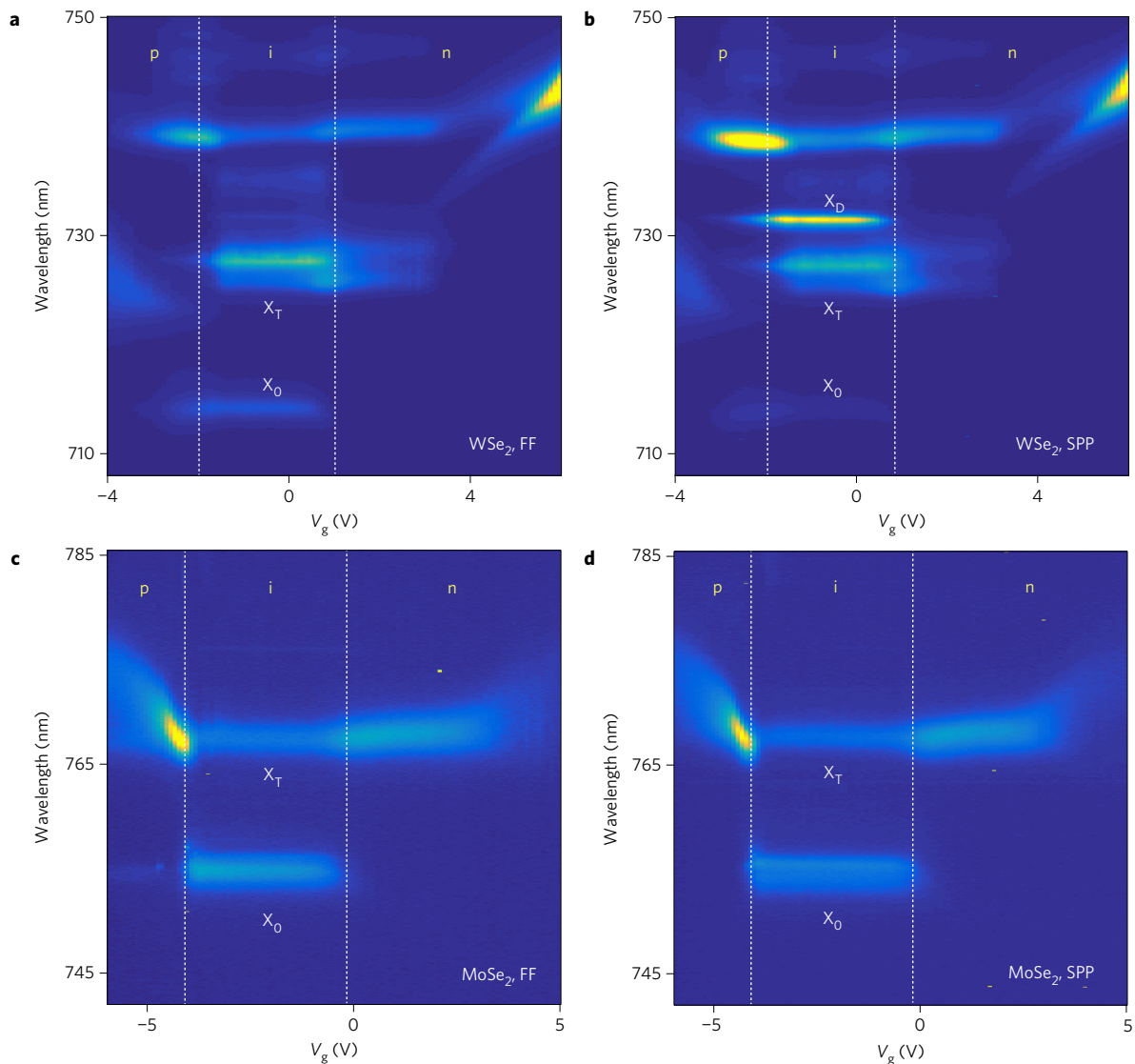
Figure 2 | Gate-dependent far-field and SPP-coupled photoluminescence spectra in WSe$_2$ and MoSe$_2$. a–d, Gate-voltage (V_g)-dependent FF-PL (**a**) and SPP-PL (**b**) spectra of WSe$_2$, and FF-PL (**c**) and SPP-PL (**d**) spectra of MoSe$_2$. The intensity is plotted on a linear scale from low (dark blue) to high (yellow). The photoluminescence intensity of **a** is normalized with respect to that of **b** (**c** is normalized with respect to **d**) so that the intensity of the charged exciton X$_T$ at zero gate voltage is equal. Dashed lines correspond to boundaries where the neutral exciton X$_O$ exists in FF-PL, and correspond to the chemical potential being inside the bandgap region (i). In **b**, a new feature X$_D$ emerges in the same V_g range as the neutral exciton. Negative (positive) gate voltages correspond to p (n) doping. The BN gate dielectric thickness is 8 nm for the WSe$_2$ sample and 10 nm for the MoSe$_2$ sample.

the normalized coupling ratio of L1 is ~3, but increases significantly and reaches a value of ~16 just when the Fermi level reaches the VB maximum ($V_g \approx -2.5$ V) and the CB minimum ($V_g \approx 0$ V). A plot of normalized coupling ratios for MoSe$_2$ does not show a comparable feature (Supplementary Fig. 7).

The origin of optical transitions with an out-of-plane dipole moment (X$_D$ and L$_1$) in WSe$_2$ can be understood by examining the band structure of monolayer TMDs. At the CB minimum and VB maximum of monolayer TMDs, that is, the K and K′ points in reciprocal space, the electronic wavefunctions can be characterized by their transformation properties under a 120° rotation (R) about the surface normal (z axis) and a reflection (P) in the TMD plane (x–y plane, Fig. 4a). Each orbital wavefunction carries a magnetic quantum number m (only m modulo 3 matters because of the reduced rotational symmetry) and a parity p (odd: $p = -1$; even: $p = 1$). Selection rules dictate that light circularly polarized in the x–y plane ($\sigma_\pm$) can only induce transitions between states with the same parity and with magnetic quantum numbers differing by one.

By contrast, light polarized linearly along the z axis couples states with opposite parity and identical magnetic quantum numbers.

Monolayer TMDs exhibit strong spin–orbit coupling proportional to **L · S**, where **L** and **S** are the orbital and spin angular momentum, respectively. The spin–orbit interaction leads to a large spin splitting in the VBs (on the order of several hundred meV[18,19]) and a much smaller splitting in the CBs. The latter is because the spin degeneracy in the CB is only lifted to second order[5,6,8] by the SOC term $L_+S_- + L_-S_+$, which mixes different orbital and spin wave functions. Notably, the splitting is of opposite sign for WSe$_2$ and MoSe$_2$ (refs 5, 6, 8) (the band orderings for WSe$_2$ and MoSe$_2$ are shown in Fig. 4b,c). Owing to the SOC mixing term, spin is no longer an exact quantum number and nominally spin-forbidden transitions, associated with dark exciton states, are in principle possible, albeit weakly. We note that the spin directions in Fig. 4b,c only denote the dominant spin direction. Two of the four possible transitions at the K point are between bands with the same dominant spin directions and are therefore optically
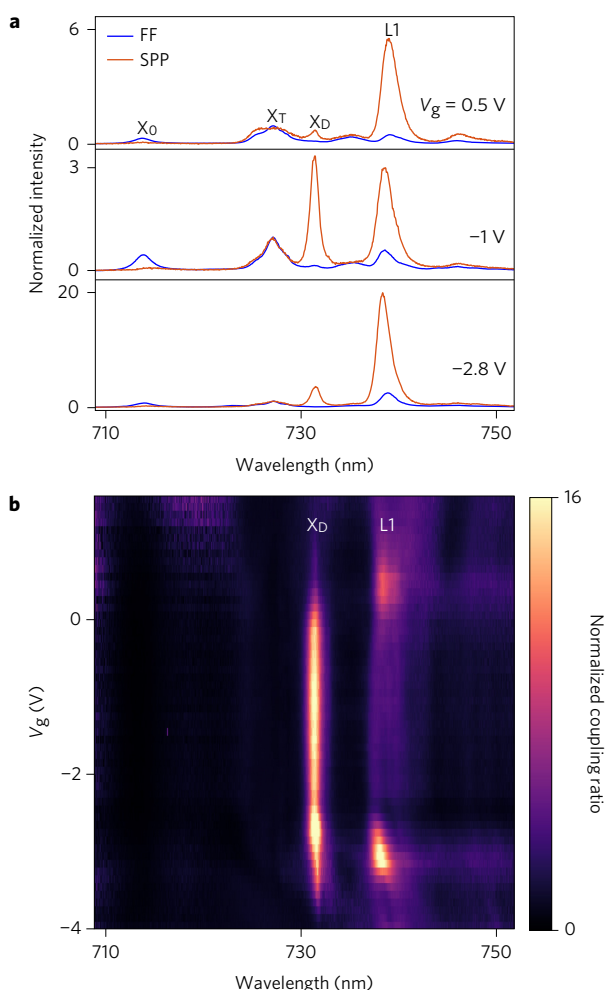
Figure 3 | Gate-dependent enhancement of the neutral and charged dark exciton state. a, FF-PL (blue) and SPP-PL (red) spectra of WSe$_2$ normalized to the intensity of the charged exciton X$_T$ at different gate voltages. X$_0$ and X$_D$ represent neutral bright and dark excitons. The L1 peak also brightens up in SPP-PL. **b**, Normalized coupling ratio, defined as the SPP-PL intensity divided by the FF-PL intensity, both normalized by the bright charged exciton intensity, as a function of gate voltage.

'bright'. For the remaining two transitions that are nominally 'dark', the transition dipole moment should be along the z direction because SOC only couples states with opposite parity. Including magnetic quantum numbers, group theoretic considerations dictate that only the transition connecting to the upper VB is allowed with z-polarized light[9,20]. The strength of the out-of-plane dipole moment is predicted to be weak, approximately a hundred times smaller than the in-plane bright exciton dipole moment[9]. However, because the energy scale associated with the sample temperature (~0.4 meV at 4 K) is much smaller than the bright/dark exciton energy splitting of ~40 meV, the exciton population at thermal equilibrium is almost entirely in the dark exciton state[7] and the dark exciton emission should be visible as long as the z-polarized light can be collected, as in the case of SPP-PL.

These band structure and SOC considerations strongly suggest that the X$_D$ feature we observe in SPP-PL of WSe$_2$ (Figs 2b and 3), with its z-polarized dipole orientation, corresponds to the dark exciton described in Fig. 4b. In contrast, in MoSe$_2$ SPP-PL (Fig. 2d), the corresponding feature is absent (Supplementary Figs 2 and 7), because the dark exciton has a higher energy than the bright exciton[5–8,21] and thus should not be observed in our experiment. We note that the X$_D$ feature in WSe$_2$ lies 42 meV below the bright exciton transition (X$_0$), similar to recently observed dark excitons[22,23] under the application of a large (up to 30 T) in-plane magnetic field. The small difference in bright/dark exciton energy splitting (42 meV in our case versus 47 meV in magnetic-field studies[22,23]) probably originates from different experimental conditions that can modify the dielectric environment and the band structure of WSe$_2$ (refs 24,25): hBN encapsulated WSe$_2$ on top of silver in our measurements versus unpassivated WSe$_2$ on SiO$_2$ (refs 22,23).

The emergence of L1, a z-polarized transition outside the bandgap region, may indicate the formation of dark charged excitons. Once the Fermi level reaches the band edge of either the CB or VB, features corresponding to the bright and dark neutral excitons disappear, suggesting that these neutral excitons bind with free carriers to form charged excitons (trions[26,27] or polarons[28]). The peak L1 may thus originate from charged dark excitons that form when neutral dark excitons bind with free electrons and holes. It should be noted that similar suggestions have been made using the observation of L1 brightening under an in-plane magnetic field[22]. The band structure of WSe$_2$ dictates that a dark charged exciton should form through the binding of a dark neutral exciton
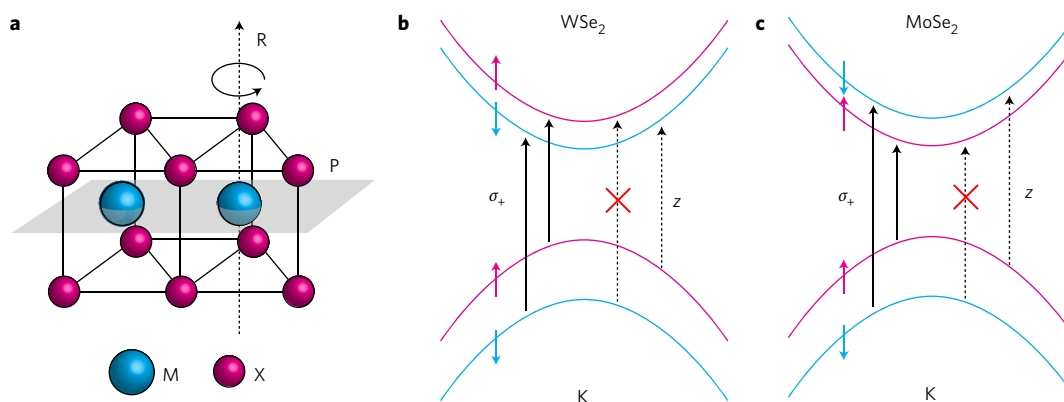

Figure 4 | Band structure and optical transitions in WSe$_2$ and MoSe$_2$ in the presence of spin–orbit coupling. a, Crystal structure of TMDs (MX$_2$) and two of its symmetries (three-fold rotation axis R and reflection plane P). **b,c**, Allowed transitions at the K point for WSe$_2$ (**b**) and MoSe$_2$ (**c**). For the K valley, the allowed transition (black solid arrow) is circularly polarized (σ^+). Coloured arrows indicate the dominant direction of the electronic spin. Due to spin–orbit coupling, spin is not an exact quantum number. In WSe$_2$ (**b**), the spin-flip transition between the upper VB and the lower CB is weakly allowed and has a transition dipole polarized in the out-of-plane (z) direction. The transition between the lower VB and the upper CB is strictly dipole forbidden. In MoSe$_2$ (**c**), the spin splitting of the CB is opposite, leading to different band ordering.

with an electron/hole in the other valley. Bright charged excitons are formed, on the other hand, by the binding of a bright neutral exciton with an electron/hole from the same or opposite valley[29]. Figure 3b also shows significant brightening of the L1 feature as the Fermi level reaches the VB maximum ($V_g \approx -2.5$ V) and the CB minimum ($V_g \approx 0$ V): this observation may suggest the reorientation of a transition dipole moment at those points or alternatively a change in the relative population of states with in-plane versus out-of-plane transition dipole moments. The exact reasons for the observation is not understood at the moment, and requires further experimental and theoretical analyses.

We have demonstrated a new method for SPP-assisted near-field spectroscopy that enables measurement of the dipole orientation of two-dimensional excitons. The technique does not require a high magnetic field and can be easily integrated with other devices, making it easily accessible, versatile and technologically relevant. We use this method to observe nominally spin-forbidden dark excitonic states in monolayer WSe_2 with out-of-plane dipole orientation, thus directly probing the SOC physics in TMD monolayers.

Our method opens up avenues for controlling the fundamental properties of atomically thin materials and the realization of new potential applications. It should enable detailed studies of indirect dark excitons[30] and the interaction between out-of-plane excitons and phonons in van der Waals heterostructures[31]. Due to the negligible coupling to free-space electromagnetic modes, the near-field coupling to tightly confined nanophotonic and plasmonic modes should play the dominant role in radiative interactions of dark excitons under a wide variety of experimental conditions. These can be used to realize active metasurfaces based on spatial modulation of exciton lifetimes and to explore schemes for chiral photonics[10] and quantum optics[11]. Finally, the dark excitons can have a long lifetime[7,9], which may be used to study transport and electrostatic manipulation of excitonic matter in two-dimensional systems[28,32,33], with potential applications for information processing and on-chip communication.

Methods

Methods and any associated references are available in the online version of the paper.

References

1. Splendiani, A. *et al.* Emerging photoluminescence in monolayer MoS_2. *Nano Lett.* **10,** 1271–1275 (2010).
2. Mak, K. F., Lee, C., Hone, J., Shan, J. & Heinz, T. F. Atomically thin MoS_2: a new direct-gap semiconductor. *Phys. Rev. Lett.* **105,** 136805 (2010).
3. Xia, F., Wang, H., Xiao, D., Dubey, M. & Ramasubramaniam, A. Two-dimensional material nanophotonics. *Nat. Photon.* **8,** 899–907 (2014).
4. Xu, X., Yao, W., Xiao, D. & Heinz, T. F. Spin and pseudospins in layered transition metal dichalcogenides. *Nat. Phys.* **10,** 343–350 (2014).
5. Liu, G.-B., Shan, W.-Y., Yao, Y., Yao, W. & Xiao, D. Three-band tight-binding model for monolayers of group-VIB transition metal dichalcogenides. *Phys. Rev. B* **88,** 085433 (2013).
6. Kośmider, K., González, J. W. & Fernández-Rossier, J. Large spin splitting in the conduction band of transition metal dichalcogenide monolayers. *Phys. Rev. B* **88,** 245436 (2013).
7. Zhang, X.-X., You, Y., Zhao, S. Y. F. & Heinz, T. F. Experimental evidence for dark excitons in monolayer WSe_2. *Phys. Rev. Lett.* **115,** 257403 (2015).
8. Kormányos, A. *et al.* K·p theory for two-dimensional transition metal dichalcogenide semiconductors. *2D Mater.* **2,** 022001 (2015).
9. Echeverry, J. P., Urbaszek, B., Amand, T., Marie, X. & Gerber, I. C. Splitting between bright and dark excitons in transition metal dichalcogenide monolayers. *Phys. Rev. B* **93,** 121107 (2016).
10. High, A. A. *et al.* Visible-frequency hyperbolic metasurface. *Nature* **522,** 192–196 (2015).
11. Poem, E. *et al.* Accessing the dark exciton with light. *Nat. Phys.* **6,** 993–997 (2010).
12. Chance, R. R., Prock, A. & Silbey, R. in *Advances in Chemical Physics* Vol. 37 (eds Prigogine, I. & Rice, S. A.) 1–65 (Wiley, 1978).
13. Gontijo, I. *et al.* Coupling of InGaN quantum-well photoluminescence to silver surface plasmons. *Phys. Rev. B* **60,** 11564–11567 (1999).
14. Wang, G. *et al.* Valley dynamics probed through charged and neutral exciton emission in monolayer WSe_2. *Phys. Rev. B* **90,** 075413 (2014).
15. Schuller, J. A. *et al.* Orientation of luminescent excitons in layered nanomaterials. *Nat. Nanotech.* **8,** 271–276 (2013).
16. Ross, J. S. *et al.* Electrical control of neutral and charged excitons in a monolayer semiconductor. *Nat. Commun.* **4,** 1474 (2013).
17. Wang, Z., Shan, J. & Mak, K. F. Valley- and spin-polarized Landau levels in monolayer WSe_2. *Nat. Nanotech.* **12,** 144–149 (2017).
18. Zhang, Y. *et al.* Direct observation of the transition from indirect to direct bandgap in atomically thin epitaxial $MoSe_2$. *Nat. Nanotech.* **9,** 111–115 (2014).
19. Zhu, Z. Y., Cheng, Y. C. & Schwingenschlögl, U. Giant spin–orbit-induced spin splitting in two-dimensional transition-metal dichalcogenide semiconductors. *Phys. Rev. B* **84,** 153402 (2011).
20. Slobodeniuk, A. O. & Basko, D. M. Spin–flip processes and radiative decay of dark intravalley excitons in transition metal dichalcogenide monolayers. *2D Mater.* **3,** 035009 (2016).
21. Wang, G. *et al.* Spin–orbit engineering in transition metal dichalcogenide alloy monolayers. *Nat. Commun.* **6,** 10110 (2015).
22. Zhang, X.-X. *et al.* Magnetic brightening and control of dark excitons in monolayer WSe_2. *Nat. Nanotech.* http://dx.doi.org/10.1038/nnano.2017.105 (2017).
23. Molas, M. R. *et al.* Brightening of dark excitons in monolayers of semiconducting transition metal dichalcogenides. *2D Mater.* **4,** 021003 (2017).
24. Komsa, H.-P. & Krasheninnikov, A. V. Effects of confinement and environment on the electronic structure and exciton binding energy of MoS_2 from first principles. *Phys. Rev. B* **86,** 241201 (2012).
25. Chernikov, A. *et al.* Exciton binding energy and nonhydrogenic Rydberg series in monolayer WS_2. *Phys. Rev. Lett.* **113,** 076802 (2014).
26. Mak, K. F. *et al.* Tightly bound trions in monolayer MoS_2. *Nat. Mater.* **12,** 207–211 (2013).
27. Ganchev, B., Drummond, N., Aleiner, I. & Fal'ko, V. Three-particle complexes in two-dimensional semiconductors. *Phys. Rev. Lett.* **114,** 107401 (2015).
28. Sidler, M. *et al.* Fermi polaron–polaritons in charge-tunable atomically thin semiconductors. *Nat. Phys.* **13,** 255–261 (2017).
29. Yu, H., Liu, G.-B., Gong, P., Xu, X. & Yao, W. Dirac cones and Dirac saddle points of bright excitons in monolayer transition metal dichalcogenides. *Nat. Commun.* **5,** 3876 (2014).
30. Rivera, P. *et al.* Observation of long-lived interlayer excitons in monolayer $MoSe_2$–WSe_2 heterostructures. *Nat. Commun.* **6,** 6242 (2015).
31. Jin, C. *et al.* Interlayer electron–phonon coupling in WSe_2/hBN heterostructures. *Nat. Phys.* **13,** 127–131 (2017).
32. Nandi, D., Finck, A. D. K., Eisenstein, J. P., Pfeiffer, L. N. & West, K. W. Exciton condensation and perfect Coulomb drag. *Nature* **488,** 481–484 (2012).
33. Fogler, M. M., Butov, L. V. & Novoselov, K. S. High-temperature superfluidity with indirect excitons in van der Waals heterostructures. *Nat. Commun.* **5,** 4555 (2014).
34. Zomer, P. J., Guimarães, M. H. D., Brant, J. C., Tombros, N. & van Wees, B. J. Fast pick up technique for high quality heterostructures of bilayer graphene and hexagonal boron nitride. *Appl. Phys. Lett.* **105,** 013101 (2014).

Author contributions

H.P., P.K., M.D.L., A.A.H., Y.Z., A.D and L.A.J. conceived the study and Y.Z., G.S., A.A.H., A.D., L.A.J., K.P. and A.Y.J. developed the fabrication procedure. Y.Z., G.S., A.A.H., A.D., C.S. and K.D.G. performed experiments and T.T. and K.W. performed hBN growth. D.S.W. and A.A.H. performed computational analyses and simulations. D.S.W., M.D.L. and H.P. contributed to theoretical descriptions. Y.Z., G.S., D.S.W., A.A.H., P.K., M.D.L. and H.P. wrote the manuscript, with extensive input from all authors.

Additional information

Supplementary information is available in the online version of the paper. Reprints and permissions information is available online at www.nature.com/reprints. Publisher's note: Springer Nature remains neutral with regard to jurisdictional claims in published maps and institutional affiliations. Correspondence and requests for materials should be addressed to P.K., M.D.L. and H.P.

Competing financial interests

The authors declare no competing financial interests.

Methods

Single-crystal silver films (250 nm thick) were grown via sputtering on the (0001) face of 4H-SiC substrates at 350 °C with a buffer layer of Ti (90 nm thick), grown at 500 °C. Typical silver films show a root-mean-square roughness of less than 1 nm and exhibit a long propagation length for SPPs[10]. Trenches that served as in- and out-coupling structures for SPPs were made using electron-beam lithography and argon ion etching. Thin layers of hBN and monolayers of WSe_2 and $MoSe_2$ were mechanically exfoliated from bulk crystals onto Si wafers coated with 285-nm-thick SiO_2. Monolayer TMDs were then identified under an optical microscope and verified via photoluminescence measurements. The thicknesses of hBN layers were measured by atomic force microscopy. The hBN/TMD/hBN heterostructures were then assembled and transferred by a dry transfer method[34] onto the patterned single-crystal silver substrates. Afterwards, thin layers of SiN (160 nm; via

plasma-enhanced chemical vapour deposition at room temperature) and alumina (30 nm; via atomic layer deposition at 90 °C) were deposited, with the pattern defined by electron-beam lithography. These served as an insulating barrier between the silver substrate and the electrical contacts to the TMDs. Finally, electrical contacts were deposited by electron-beam evaporation of Cr (10 nm)/Au (90 nm) followed by sputtering of another 40 nm of Au, with the dimensions defined by electron-beam lithography. Optical measurements were carried out in a home-built confocal microscope using an objective with a numerical aperture of 0.75 in a 4 K cryostat (Montana Instruments). Two galvo mirrors were used to scan the excitation and collection spots independently on the sample.

Data availability. The data that support the plots within this paper and other findings of this study are available from the corresponding author upon reasonable request.